Estuarine, Coastal and Shelf Science 258 (2021) 107423

Contents lists available at ScienceDirect

Estuarine, Coastal and Shelf Science

journal homepage: www.elsevier.com/locate/ecss

Sedimentary signatures of the abrupt deglacial rise in sea level from the East China Sea inner shelf

Fengming Chang [a,b,d], Tiegang Li [b,c,*], Lihua Zhuang [a,b,d], Hanjie Sun [a,b,d], Zhifang Xiong [b,c], Rongtao Sun [e]

[a] Key Laboratory of Marine Geology and Environment, Institute of Oceanology, Chinese Academy of Sciences, Qingdao, 266071, China
[b] Laboratory for Marine Geology, Qingdao National Laboratory for Marine Science and Technology, Qingdao, 266061, China
[c] Key Laboratory of Marine Sedimentology and Environmental Geology, First Institute of Oceanography, SOA, Qingdao, 266061, China
[d] Center for Ocean Mega-Science, Chinese Academy of Sciences, Qingdao, 266071, China
[e] School of Resources & Environment Engineering, Shandong University of Technology, Zibo, 255049, China

ARTICLE INFO

Keywords:
Sea-level signatures
Deglacial meltwater pulses
Abrupt cooling event
East China Sea inner shelf

ABSTRACT

Understanding the link between deglacial sea-level jumps and abrupt climate change may provide crucial insights into future ice-climate feedbacks. However, much ambiguity remains surrounding many of the last deglacial meltwater pulses. Here, we present a complete sedimentary succession from the inner shelf of the East China Sea, which has clearly documented multiple abrupt rises in the deglacial sea level. The results suggest that the postglacial sedimentary sequence, resting on a late Pleistocene basement of stiff clay, formed during a three-stage process marked by characteristic lithology and foraminiferal fauna. The abrupt shifts in the sedimentary facies indicate that seawater firstly intruded into the inner shelf just before the onset of the slowdown in sea-level rise caused by the Younger Dryas cooling event and changed the inner shelf into a tidal flat environment, as demonstrated by the sudden appearance of both planktonic foraminifera and typical brackish-water species of benthic foraminifera. Meltwater pulse 1B (MWP-1B) is depicted by a sharp upward transition to a nearshore subtidal environment at 11.62 kyr. This episode of sea-level rise induced the initial flooding of the inner shelf, which is well documented by the sudden reduction in brackish-water foraminifera species and evident increase in inner-shelf benthic species. The prominent sea-level rise at approximately 7.54 kyr was responsible for the shift to stable inner shelf conditions and resulted in the maximum flooding of the inner shelf area, initiating subsequent formation of the alongshore mud wedge. Additionally, obvious peaks in both the benthic foraminifer abundance and the marine algae concentration at approximately 8.13 kyr confirm the previously identified sea-level jump at approximately 8.2 kyr, which coincides with the weakening of the Asian monsoon demonstrated by the peak grain size in our record, further indicating its apparent connection to the 8.2 kyr climatic reversal.

1. Introduction

The currently rising sea level due to polar ice mass loss and coupled atmosphere-ocean feedbacks is of great concern (Dutton et al., 2015). Unfortunately, the rate and pattern of sea-level variations under future global warming are highly uncertain in current climate models (Meyssignac et al., 2017). Reconstructions of sea-level changes during the last deglaciation have provided substantial evidence for dramatic sea-level rises and major global climate perturbations induced by catastrophic meltwater releases into the North Atlantic Ocean (Smith et al., 2011; Carlson and Clark, 2012). Hence, continuous and well-constrained records of sea-level changes associated with climate fluctuations during the last deglaciation may provide critical insights into the potential responses of climate and sea level to the accelerated melting of polar ice sheets in the context of future climate scenarios.

Numerous records have shown that the gradual rise in sea level accompanying the last deglacial warming was punctuated by several short-lived jumps (Carlson and Clark, 2012). Among these episodes of sea-level rise, only meltwater pulse 1A (MWP-1A), coined by Fairbanks (1989) to refer to the exceedingly rapid sea-level rise that occurred at approximately ~14.6 kyr BP, is relatively well constrained (Deschamps et al., 2012), although many uncertainties concerning its ice sheet

* Corresponding author. Laboratory for Marine Geology, Qingdao National Laboratory for Marine Science and Technology, Qingdao, 266061, China.
E-mail address: tgli@fio.org.cn (T. Li).

https://doi.org/10.1016/j.ecss.2021.107423
Received 6 June 2020; Received in revised form 4 May 2021; Accepted 12 May 2021
Available online 28 May 2021

source and magnitude remain (Carlson and Clark, 2012; Törnqvist and Hijma, 2012; Cuzzone et al., 2016). To date, few studies have produced a single record of sea-level changes that spans the full deglaciation and therefore completely captures all meltwater episodes. Such studies are hampered by low temporal resolution, low proxy sensitivity and strong local expressions of sea-level change, leaving considerable debate over many other deglacial meltwater pulse events (Smith et al., 2011).

In addition, many records indicate that some of the sea-level jumps during the early Holocene were likely closely linked to abrupt climate cooling events (Barber et al., 1999; Cronin et al., 2007; Kendall et al., 2008; Li et al., 2012; Törnqvist and Hijma, 2012). The catastrophic discharges of freshwater into the North Atlantic probably not only induced sea-level rise but also weakened the Atlantic meridional overturning circulation (AMOC) and cooled the global climate (e.g., Tornqvist and Hijma, 2012). Nevertheless, except for the sea-level signature of the "8.2 kyr climatic reversal", triggered by the final drainage of proglacial Lake Agassiz-Ojibway in North America (Kendall et al., 2008; Hijma and Cohen, 2010; Li et al., 2012), little is known about the patterns of sea-level change associated with other abrupt early Holocene climate events (Clark et al., 2001; Mitrovica et al., 2001; Peltier, 2002; Carlson and Clark, 2012). This lack of knowledge limits our understanding of the feedbacks between climate variation, ice sheet dynamics, and sea-level change within the context of ongoing global warming.

The sea-level rise following the last glacial maximum (LGM) determined the evolution of coastal depositional systems. As a shelf was quickly inundated, the coastal system and its depocenter rapidly migrated landward, forming a variety of sedimentary sequences stacked over a wide area of continental shelf. Thus, the sedimentary succession in the present coastal areas may contain details of the rapid sea-level change during the deglacial transgression. The broad shelf region of the East China Sea (ECS) is of particular interest since it is highly sensitive to past sea-level changes, owing to its low gradient and large sediment inputs from the Yangtze River. These features make it an ideal site to determine the sea-level jumps and abrupt climate changes related to meltwater release events during the last deglaciation.

Early studies on the nearshore and submerged western Pacific continental shelves have identified multiple deglacial meltwater pulses based on the synthesis of extensive sea-level indicators from the ECS, Yellow Sea and Sunda Shelf (Liu and Milliman, 2004; Liu et al., 2004). Although studies in the ECS and adjacent areas have also reported evidence of some sporadic rapid sea-level rises during the last deglaciation (e.g., Liu et al., 2010, 2020; Chang et al., 2015), the validity of these events in this area still awaits further confirmation. Moreover, their potential links to abrupt climate changes have not been thoroughly scrutinized in the existing studies. In this paper, we investigate a new sedimentary sequence from the last deglaciation on the ECS inner shelf. Our main objective is to trace the major deglacial events of abrupt sea-level rise in the area based on sedimentary facies transitions with a focus on the sea-level signatures of abrupt cooling events during the early Holocene.

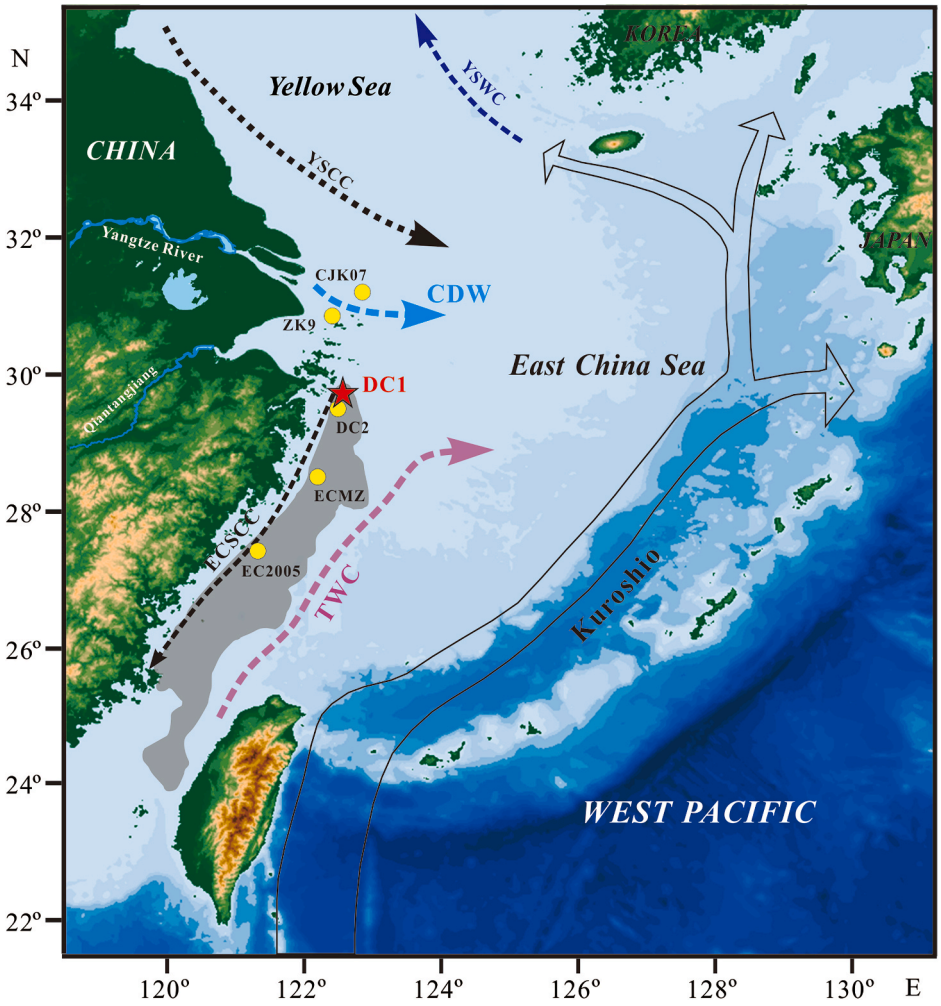

Fig. 1. Schematic illustration of the bathymetry and surface circulation patterns in the East China Sea and adjacent seas. The dark gray shaded area represents the distribution of the mud wedge in the ECS inner shelf. The locations of core DC1 and other cores mentioned in the text are marked by stars and dots, respectively. The circulation patterns are based on previous studies (Lie and Cho, 2016). YSWC: Yellow Sea Warm Current, YSCC: Yellow Sea Coastal Current, CDW: Changjiang Diluted Water, ECSCC: East China Sea Coastal Current, TWC: Taiwan Warm Current. (For interpretation of the references to color in this figure legend, the reader is referred to the Web version of this article.)

2. Regional setting

As a typical marginal sea located between the western Pacific Ocean and East Asia (Fig. 1), the ECS is characterized by a broad continental shelf and high levels of fluvial discharge, particularly from the Yangtze River. Postglacial sea-level changes and climate fluctuations have exerted significant influences on the coastal hydrological regime and therefore the hydrodynamic systems, which have controlled the development of late Quaternary depositional sequences on the ECS shelf (Hori and Saito, 2007; Xu et al., 2012). Meanwhile, the riverine discharge to the ECS is largely influenced by East Asian summer monsoon (EASM) precipitation, which was responsible for the supply of sediment to the ECS and accordingly influenced the deposition of Yangtze-derived sediments on the ECS inner shelf during the last deglaciation (Liu et al., 2007a; Xu et al., 2016).

After the postglacial sea level reached its maximum along the southeastern coast of China during the middle Holocene at approximately 7.5 kyr BP (e.g., Zong et al., 2004; Li et al., 2014; Xue, 2014), the modern Chinese coastal current system is believed to have developed gradually into its present pattern (Li et al., 2002; Liu et al., 2010) and has since played a critical role in the dispersal and deposition of riverine sediments on the shelf. Currently, the ECS shelf circulation predominately consists of seasonal, counterclockwise circulation (Lie and Cho, 2016) (Fig. 1). During the summer months when the ECS is dominated by the southwest monsoon with large river discharges, the southward-flowing ECS Coastal Current (ECSCC) along the Chinese coast is quite weak. Much of the Yangtze-delivered sediment is temporarily confined to the river mouths. Conversely, the Taiwan Warm Current (TWC), which flows northeastward over the middle shelf, markedly intensifies in response to the prevailing southeast monsoon, confining the Yangtze-delivered sediments to the inner shelf (Lee and Chao, 2003). However, a surface plume known as Changjiang diluted water (CDW) forms due to a northeastward extension of Yangtze runoff and transports a small amount of suspended sediment to the outer shelf. During the winter, the ECSCC dramatically strengthens under the vigorous northeast monsoon (Lie and Cho, 2016). Although the Yangtze discharge is significantly reduced, a large quantity of fine-grained sediments is transported southward and trapped on the inner shelf, forming an elongated mud wedge off the Zhejiang-Fujian coast (Fig. 1). This distal subaqueous mud wedge is clearly differentiated from the sand- and silt-dominated deposits of the middle and outer shelf (Liu et al., 2007a; Xu et al., 2012).

3. Material and methods

CHIRP seismic profiles and sedimentological investigations show that an elongated mud wedge extends approximately 1000 km from the Yangtze mouth southward into the Taiwan Strait along the ECS inner shelf (Liu et al., 2007a; Xu et al., 2012). To penetrate this clinoform deposit with a >40-m-thick depocenter and reach its basal strata, borehole DC1 was drilled on its northern edge off the Zhejiang-Fujian coast at a water depth of 28 m (122°30′48°E, 29°40′11°N) in 1979 (Fig. 1). The core is 26.9 m long, but the top 6.8 m sediments are missing owing to poor core recovery. The core sequence is characterized by a basal unit comprising uniform stiff clay with an erosional surface at a core depth of 24 m. This distinct, late Pleistocene basement is overlain by a transgressive fine sand layer. Within this section, a thin, basal peat layer is observed at a core depth of 21.92–21.96 m. Separated by a shell fragment-rich layer on top of the fine sandy sediments, the upper section of the core between 6.8 and 18.9 m is composed of alternating homogeneous fine silty clay and clayey silt with sporadic shell debris and silt lenses (Fig. 2). The core was split, described, and subsampled in the laboratory in the early 1980s. In this study, 131 and 165 subsamples from the 6.8–25.35 m section of the core were collected according to the downcore lithology variations in grain size and foraminifera, respectively.

For grain-size analysis, after drying at ~40 °C, well-mixed bulk samples were pretreated with 10% H_2O_2 and 0.1 N HCl to remove organic matter and biogenic carbonate, respectively. Then, the samples were treated with 0.5 N sodium polyphosphate and further dispersed in an ultrasonic oscillator. The grain sizes of the remaining detrital materials were determined using a Cilas940 L laser diffraction particle analyzer, with a measurement range of 0.3–2000 μm. The repeated measurement error was within 2%. The clay (<4 μm), silt (4–63 μm),

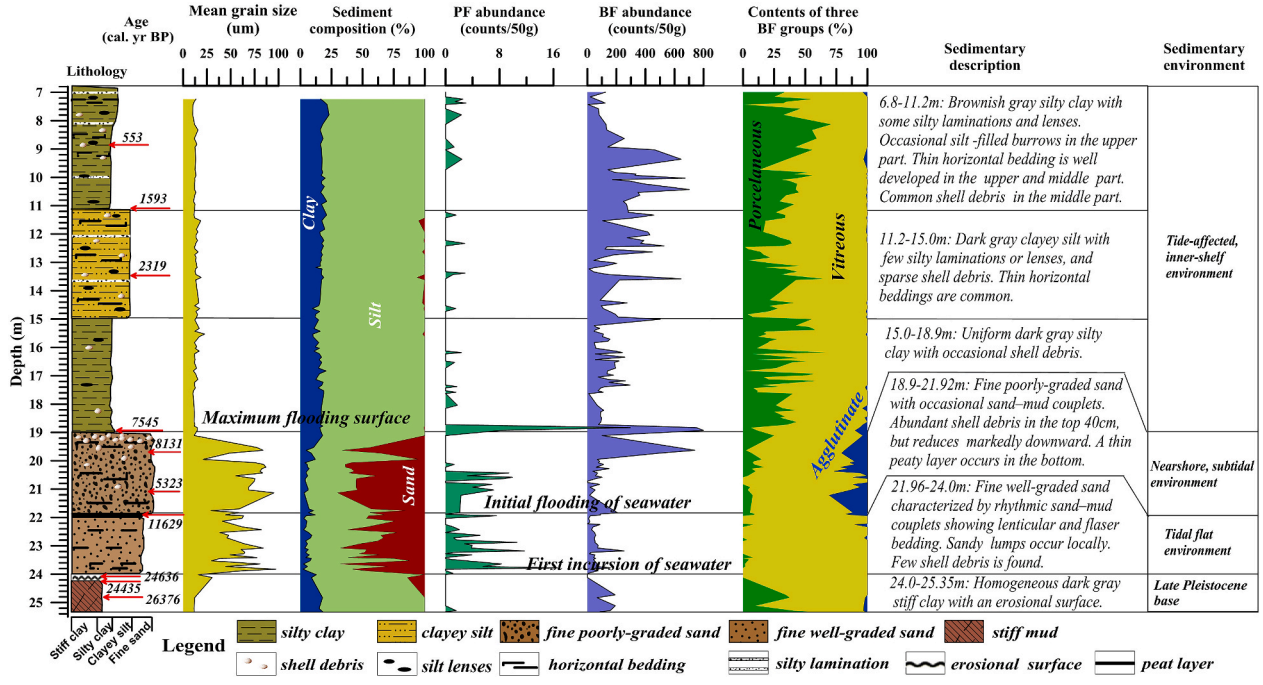

Fig. 2. Composite depth profile of core DC1 showing the lithology, calibrated age, mean grain size, sediment composition, foraminifera abundance, composition of benthic foraminifera, and interpretation of sedimentary facies. PF: planktonic foraminifera, BF: benthic foraminifera.

and sand (63–2000 μm) fractions were calculated from the cumulative grain size distributions based on volume proportions.

Samples for foraminifera analyses were first dried at ~40 °C, then soaked in distilled water for 36 h. After rinsing through a 63 μm sieve, the dried fractions over 63 μm were examined under a stereoscopic microscope. For samples with abundant foraminifera tests, at least 200 tests were identified and counted. However, in samples with fewer foraminifera tests, all specimens in the coarse fractions were counted. Both the planktonic and benthic foraminifera abundances were calculated on the basis of a dry sample size of 50 g.

Accelerator mass spectrometry (AMS) ^{14}C dates of three samples were measured on well-preserved calcareous tests of mixed benthic foraminifer species. Bivalve and gastropod molluscan shells or shell debris from three other samples were dated due to a lack of foraminifera tests. Moreover, three organic sediment samples were dated since materials suitable for ^{14}C dating are unavailable in the lower part of core DC1. Of these AMS ^{14}C dates, one was measured at the National Ocean Sciences Accelerator Mass Spectrometry (NOSAMS) facility, USA, and the eight others were determined at Beta Analytic Inc., USA. (Table 1).

In addition, to determine the age of the basal peat layer in core DC1, one previously reported peat ^{14}C date from core DC2 was employed because of the unavailability of peat samples in our core, which were exhausted in previous work (Sun et al., 1989). Core DC2 was also obtained from a site in the inner-shelf mud wedge that is only 11 km southwest of the DC1 core site with the same water depth (Fig. 1). The peaty layer in core DC1 is well correlated to that in core DC2 according to their sedimentary successions (Fig. S1).

All ^{14}C dates of the calcareous and organic materials were calibrated using the online program Calib 8.20 (Stuiver et al., 2021) with the calibration data set of Marine20.14c or IntCal20.14c (Heaton et al., 2020; Reimer et al., 2020). A local reservoir age (ΔR) of −127 ± 70 yr was used based on 17 ages obtained around the ECS (Yoneda et al., 2007; Hirabayashi et al., 2017) for all marine shell samples. Furthermore, the radiocarbon age from the basal peat layer was indicated by only the ^{14}C age (Sun et al., 1989). It was also calibrated to 2σ median age using Calib 8.20 based on the IntCal20.14c calibration data set. The calibrated ages are expressed as calendar ^{14}C ages before the present (AD 1950) with 2σ uncertainties (Table 1).

To trace the sedimentary successions along the inner shelf of the ECS, stratigraphic data compiled from five published sediment cores were also collected (Fig. 1, Table S1). The detailed lithological characteristics, sedimentary structures, fossil components and sedimentary facies of each core have been described previously (Wang et al., 2010; Xu et al., 2012, 2016, 2016; Dong et al., 2018). Thirty-nine previously reported ^{14}C dates obtained from molluscan shells, foraminifera, plant materials, and sedimentary organic matter in the cores were also collected (Table S2).

4. Sedimentary facies successions

High-resolution seismic profiles depict several acoustic units within the inner-shelf mud wedge (Liu et al., 2007a; Xu et al., 2012, 2016). The lower parts of the seismic profiles display a prominent reflector that truncates the underlying strata. Multiple internal reflections prevail in the area, and a distinct subsurface reflector, overlain by a thick clinoform, can be observed in most seismic profiles within the mud wedge (Liu et al., 2007a; Xu et al., 2012). The sediment in the basal section (25.35–24.0 m) of core DC1 is composed of homogeneous stiff clay with dispersed reddish-brown oxidized spots. This section consists mainly of silt (77.0%–86.9%), followed by clay (8.9–17.9%) and sand (0–14.0%), with a mean grain-size range of 16.0–11.4 μm (Fig. 2). The stiff clay layer is widely distributed across the adjacent Yangtze Delta and can be traced across the ECS shelf (Fig. S1). This unit was previously believed to have formed on the paleo-interfluve of the Yangtze River during the last glacial sea-level lowstand as a result of long-term exposure to coastal-fluvial sediments. This stiff clay layer also corresponds well to a major truncation surface in the seismic profiles and represents the late Pleistocene basement in the ECS shelf areas (Li et al., 2002; Wang et al., 2010; Xu et al., 2016).

Benthic foraminifera are relatively abundant in the basal section (66–190 grains/50 g of dry sediments) and mainly comprise offshore shallow sea species with both vitreous and porcelaneous shells, indicating that this unit was mainly of marine origin (Fig. 2) (Wang et al., 1985; Li et al., 2002). Furthermore, the absence of planktonic foraminifera and the presence of fine-grained sediment suggest that the material in this section was originally deposited in a littoral and neritic environment, since planktonic foraminifera are most abundant in the far middle and outer shelf in areas deeper than 50 m in the ECS (Wang et al., 1985). However, the dispersed, oxidized stains, combined with seriously worn shells of benthic foraminifera, indicate that the stiff clay layer was once exposed and experienced weathering. This deduction is further corroborated by the presence of an erosional surface at the top of this section with a calibrated ^{14}C age of 24.6 kyr BP, implying an LGM sea-level lowstand on the ECS shelf (Fig. 2).

The sediments overlying the basal stiff clay layer are obviously coarser, with an average mean grain size of 59.7 μm, and comprise 12.0–67.8% sand, 28.8–80.1% silt, and only 2.3–9.1% clay (Fig. 2). This section (24.0–21.96 m) is characterized by typical sand-clay couplets with well-developed rhythmic horizontal lamination, which is accurately documented by the alternating increase in sand and silt contents in the sediment composition (Fig. 2). Such a sedimentary structure suggests that the deposits were strongly influenced by tides, as sand-clay couplets typically form in tidal flat systems (Hori et al., 2001). A strong tidal signal is also supported by the persistent occurrence of planktonic foraminifera, despite the deficiency in shell debris and inner-shelf benthic species (Figs. 2 and 3), since seawater overflow caused by a strong tide can transport planktonic foraminifera several tens of kilometers landwards on the present ECS shelf. The benthic foraminiferal fauna is dominated by typical brackish-water species, including *Ammonia beccarii* var., *A. dominicana* and *Cribrononion subincertum,* with a notably high percentage of 54–85% (Fig. 3). These species are well known for their tolerance to salinity fluctuations (Murray, 2006; Langer

Table 1
^{14}C and calibrated ages for core DC1.

Lab. code	Sample depth (m)	δ^{13}C (‰)	Conventional age (^{14}C yr BP)	Calibrated age (cal. yr BP)		Dated materials
				median age	2σ age range	
Beta-394471	8.84	−0.8	1000 ± 30	553	379–715	Benthic foraminifera
OS-101063	11.18	0.31	2050 ± 20	1593	1379–1807	Benthic foraminifera
Beta-394474	13.53	NA	2640 ± 30	2319	2078–2601	Benthic foraminifera
Beta-429368	18.93	1.5	7130 ± 30	7545	7357–7734	Bivalve mollusc shell fragments
Beta-409628	19.73	−1.1	7720 ± 30	8131	7939–8334	Gastropod shell
Beta-394476	21.13	NA	5030 ± 30	5323	5064–5546	Bivalve mollusc shell fragments
*	21.94	NA	10250 ± 100	11629	11255-11972	Peat
Beta- 512612	24.02	−20.3	20550 ± 60	24636	24316-24915	Organic sediment
Beta- 530313	24.13	−19.5	20420 ± 60	24435	24203-24657	Organic sediment
Beta- 530314	24.73	−20.4	22230 ± 80	26376	26015-26525	Organic sediment

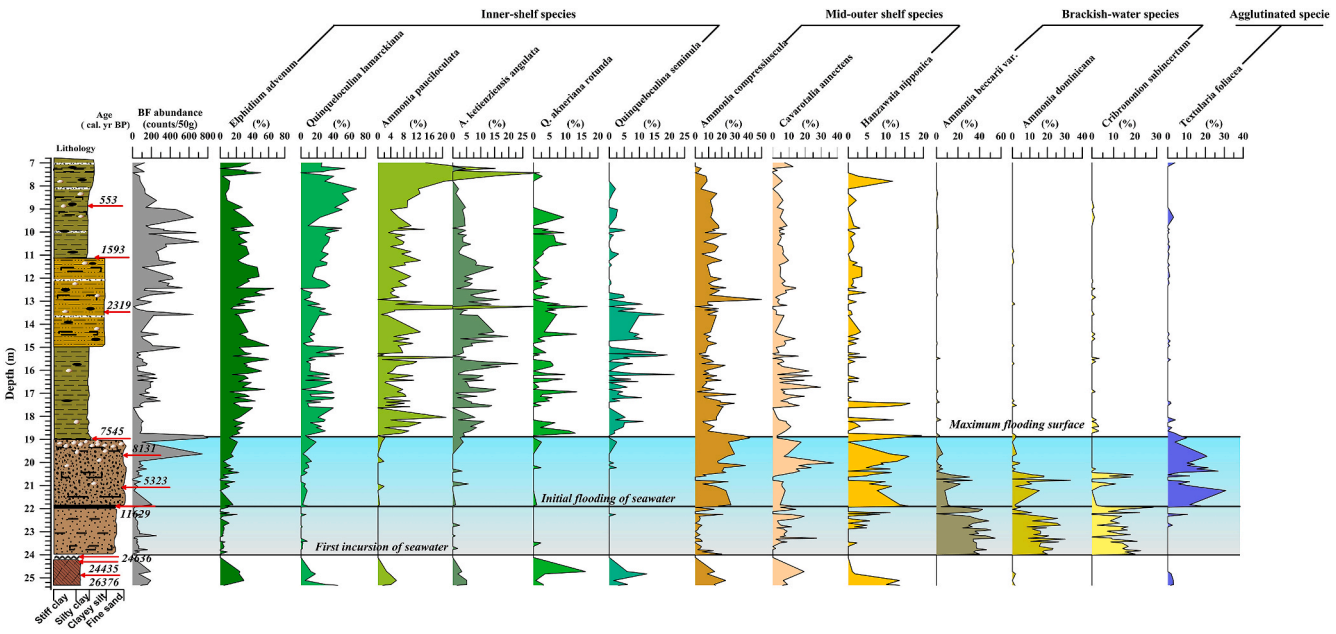

Fig. 3. Downcore variations in the abundance of benthic foraminifera and percentages of the common benthic foraminifera species in core DC1. The legend for the lithology and sedimentary structures is the same as that in Fig. 2. BF: benthic foraminifera.

et al., 2013) and are the most common benthic foraminifera in the upper intertidal zone off the modern Yangtze estuary (Wang et al., 1985; Liu et al., 2010). Most of the littoral to shelf species in the present ECS (such as *A. pauciloculata*, *A. ketienziensis angulate*, *A. compressiuscula*, *Quinqueloculina lamarckiana*, *Q. akneriana rotunda* and *Q. seminula*) occur sporadically, with commonly low percentages in this unit. The benthic foraminifera assemblages suggest that a coastal tidal flat environment prevailed in this interval. In fact, tidal flat facies are widely found in most of the cores from the adjacent subaqueous Yangtze Delta, which developed before seawater inundated the study area (Xu et al., 2016). Therefore, this tidal flat facies represents the first incursion of seawater to the ECS inner shelf during the period of postglacial sea-level rise.

Separated by a thin peat layer at a core depth of 21.96–21.92 m (Fig. 2), the coastal tidal flat deposits pass upward into poorly graded, fine sands (3.0–12.0% clay, 26.9–83.1% silt, and 14.7–70.0% sand) with an average mean grain size of 67.6 μm. The interval (21.92–18.90 m) is distinguished by substantial changes in the foraminiferal fauna, including the abrupt appearance of agglutinated benthic foraminifera and a distinct decline in the content of brackish-water species (Figs. 2 and 3). The agglutinated foraminifera are composed monospecifically of *Textularia foliacea*, which is a common species in shallow waters and is mainly found in the middle shelf of the modern ECS (Wang et al., 1985). Its dominance indicates that the core site prevailed under turbulent open ocean conditions, which corresponds well to the coarse grain size. Notably, the abundance of brackish-water species markedly decreased moving upward in this section, indicating an enhanced marine influence caused by sea-level rise. This increasing influence of marine conditions is also clearly evidenced by the perceptible increase in the percentage of inner-shelf species and porcelaneous tests of benthic foraminifera, implying increases in salinity and water depth (Wang et al., 1985). Meanwhile, the substantial influence of tides is evidenced by the persistent presence of planktonic foraminifera combined with the flourishing of mid-to outer-shelf species, as typified by *Hanzawaia nipponica, Cavarotalia annectens* and *A. compressiuscula* (Fig. 3). Furthermore, locally developed sand-clay couplets in this section can be attributed to strong tidal effects. This interpretation is consistent with the coexistence of completely marine species and euryhaline species of foraminifera in the section, which are indicative of highly variable conditions (Figs. 2 and 3). It is reasonable to interpret that the interval above the peat layer represents a tidally influenced nearshore subtidal facies.

Throughout the sedimentary column, the most prominent changes in our records occurred at approximately 18.90 m, implying a pronounced shift in the sedimentary regime (Figs. 2 and 3). The lithology of the top portion of the core (18.90–6.8 m) is entirely different from that of the underlying sections and is characterized by uniform, fine silty clay or clayey silt (9.6–23.0% clay, 74.9–89.7% silt, and only 0–6.2% sand) with only occasional silty laminations, thin horizontal bedding and locally common shell debris (Fig. 2). Based on the homogeneous, fine-grained (average mean grain size of 13.15 μm) lithological composition and depositional age (younger than 7.54 kyr BP), the sediments of this section clearly correspond to the inner-shelf mud wedge, representing the highstand system tract that has accumulated since sea level reached its highest level in the middle Holocene (Liu et al., 2007a, 2010; Xu et al., 2012). Benthic foraminifera are consistently abundant in this interval (up to several hundred individuals per 50 g of dry sediments) and are overwhelmingly dominated by inner-shelf species with calcareous tests, represented by *Elphidium advenum*, *Q. lamarckiana* and *A. pauciloculata* (Figs. 2 and 3). The disappearance of brackish-water species and lack of *T. foliacea* imply increasingly marine conditions. Moreover, the sporadic appearance of planktonic foraminifera, in combination with the significant decrease in the abundance of mid-to outer-shelf benthic species, indicates that the foraminiferal fauna in this section resembles the living groups in the offshore shallow-shelf areas (<20–30 m water depth) in the ECS (Wang et al., 1985; Li et al., 2002). This section was clearly deposited in a relatively stable inner-shelf environment similar to that found today over the core site.

5. Discussion

5.1. Sedimentary imprints of deglacial rapid sea-level rise

5.1.1. The first incursion of seawater

In our core, three calibrated ages indicate that the stiff clay layer was developed during the LGM period (~26.5–19.0 kyr BP). This stiff clay layer is popularly found on the northern shelf of the ECS, resting on a set of pre-LGM coastal to fluvial deposits with abundant oxidized spots, as shown in cores ZK9 and CJK07 (Wang et al., 2010; Xu et al., 2016)

(Fig. S1). During the LGM, the dramatically falling sea level resulted in seaward progradation of the shoreline, which allowed the river drainage systems to extend their channels on the exposed ECS shelf (Saito et al., 1998; Wellner and Bartek, 2003; Ujiié et al., 2003; Li et al., 2014), as shown by the incised valleys filled by flat or inclined strata in the seismic profiles within the inner shelf (Xu et al., 2012). The majority of riverine terrigenous sediments bypassed the inner shelf, facilitating the formation of a stiff clay layer in the exposed interfluves due to long-term weathering of the pre-LGM sediments (Li et al., 2002).

The sharp transition from stiff clay to the overlying tidal flat deposits, separated by an erosional surface, implies the first incursion of seawater to the DC1 coring site (Figs. 2 and S1). The age of this boundary in our core could not be determined due to a lack of materials suitable for ^{14}C dating. However, we infer that the first incursion of seawater to core site DC1 occurred roughly between 12.76 and 13.10 kyr BP based on the sedimentary successions in well-dated cores EC2005 and ZK9, which sit at water depths slightly deeper and shallower, respectively, than our core in the inner ECS shelf (Fig. S1). This deduction is consistent with the abrupt transition from fluvial to estuarine conditions in the Yangtze River Delta at approximately 13 kyr (Liu et al., 2020). The timing was much later than the age of MWP-1A at ~14.6–14.3 kyr BP with an abrupt rise in sea level (40 mm/yr) (Fig. 4) (Deschamps et al., 2012; Lambeck et al., 2014). Although MWP-1A has apparent sedimentary signatures indicative of a depositional hiatus that occurred at 14.5–13.7 kyr BP in the deepest part of the ECS outer shelf (Wang et al., 2014), the seawater transgression promoted by it had not influenced our core site before the slowdown of sea-level rise caused by the Younger Dryas cooling event (Fairbanks, 1989; Bard et al., 2010; Abdul et al., 2016).

The incursion of seawater to the inner shelf might trigger strong tidal current action and significantly influence on the coring site, as shown by the presence of planktonic foraminifera and tide-influenced sedimentary structures in the interval of 21.96–24.0 m (Figs. 2 and 5). Strong tidal action could have facilitated erosional and reworking processes and resulted in a basal erosional surface on the top of the stiff clay layer that

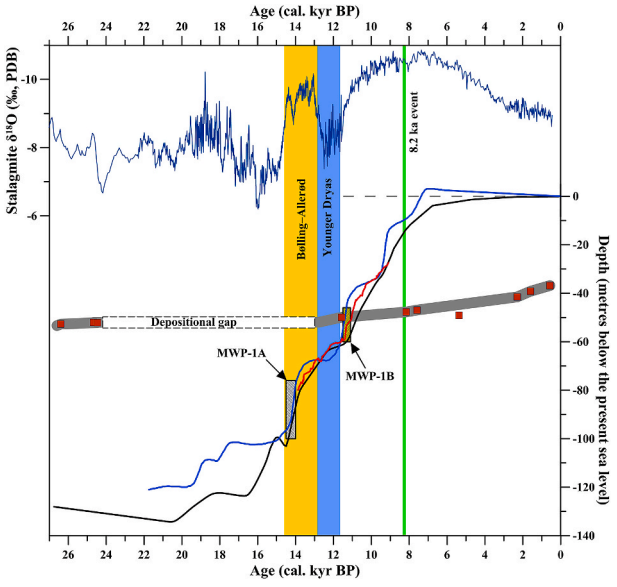

Fig. 4. Age-depth plot for core DC1 along with different sea level curves (dark line, the ice volume equivalent sea level curve of Lambeck et al. (2014); red line, the Barbados U–Th-dated sea level curve from Abdul et al. (2016); blue line, the relative sea-level change in the western Pacific proposed by Liu et al. (2004)). Additionally, composite $\delta^{18}O$ records from a Chinese stalagmite are shown (Wang et al., 2008). The vertical bars of various colors indicate the major climatic events: the Bølling–Allerød warm period, the Younger Dryas cold period and the 8.2 ka cooling event. MWP-1A and MWP-1B are meltwater pulses 1A and 1B, respectively. (For interpretation of the references to color in this figure legend, the reader is referred to the Web version of this article.)

is clearly depicted by a prominent acoustic reflector in the CHIRP seismic profiles across site DC1 reported by Liu et al. (2007a) and Xu et al. (2012) (Fig. S2). Long-term subaerial exposure and destructive erosion could have led to a long hiatus in sediment deposition at the coring site (Fig. 4). Following the incursion of seawater, a tide-dominated brackish-water environment prevailed at the coring site, as represented by the dominance of typical brackish-water species of benthic foraminifera; thus, a tidal flat system developed in the inner shelf (Figs. 3 and S1).

5.1.2. *The initial flooding of seawater*

The onset of nearshore subtidal conditions with a strong tidal influence at our core site is marked by the presence of a thin peat layer and abrupt changes in the foraminiferal fauna (Figs. 2 and 3). The basal peat layer has been widely recognized in multiple cores across the adjacent shelf regions of eastern China and represents the initial flooding surface during rapid postglacial transgression (Liu et al., 2007b, 2010, 2010; Wang et al., 2010). This initial flooding surface is well correlated to an internal bounding surface caused by a rapid landward transgression in the seismic profile across site DC1 (Liu et al., 2007a, 2020). Clearly, an early rapid flooding event terminated peat formation and converted the core sites into an open-water, brackish environment, as shown by the foraminifera composition (Fig. 3). This major sea-level jump is further evidenced by the synchronous sudden emergence of marine algae in the studied core, which was otherwise absent after the first incursion of seawater (Fig. 5), since an intensive marine influence would facilitate the survival and growth of marine algae because of their high salinity tolerance.

Abrupt sea-level rise during the early Holocene, referred to as MWP-1B, has been previously reported at various locations (Blanchon and Shaw, 1995; Liu and Milliman, 2004). However, there is considerable debate as to its existence, since no evidence of significant sea-level rise has been detected in most of the coral and nonreef records in support of a well-defined MWP-1B (Braithwaite, 2016; Dong et al., 2018). Changes in relative sea level could be caused by a combination of eustatic, hydro-isostatic and local tectonic processes. The East China coast, which is far from the boundary of the Philippine Plate (~900 km) with an extensive and temperate continental shelf, has been tectonically stable over Quaternary times (Chen and Stanley, 1995; Zang et al., 2016). Furthermore, it is generally accepted that the impacts of glacial isostatic adjustment (GIA) were only negligible at this far-field site, considering the much smaller amplitude of hydro-isostatic effects on sea-level change (a few meters) than that of the MWP-1B (Milne and Mitrovica, 2008; Stanford et al., 2011; Yusuke et al., 2018; Tian et al., 2020). In our records, the comparable peat layer in neighboring core DC2 yields a calibrated age of 11.62 kyr BP, which is similar to the timing of MWP-1B proposed by most authors (Blanchon and Shaw, 1995; Liu and Milliman, 2004; Abdul et al., 2016; Tian et al., 2020). This age is also in accord with the sudden initiation of incised-valley-fill systems in most of the river deltaic basins in East Asia, indicating widespread rapid flooding of the shelf lowlands (Hori et al., 2001). Therefore, it is considered that the sharp transition of the depositional environment in our records reflects the MWP-1B event. This finding is consistent with the records of a clear flooding surface in the clinoform stratigraphy from the northern Yellow Sea and an abrupt change from an estuarine-to tide-dominated shelf off the present Yangtze River estuary (Liu et al., 2007b, 2020). Additionally, our conclusion is further corroborated by the sharp transition in the sedimentary environment along most of the cores from the ECS inner shelf (Liu et al., 2010; Wang et al., 2010; Dong et al., 2018) (Fig. S1).

Based on the core depth of 21.96 m, where MWP-1B registered at site DC1 at a water depth of 28 m, the relative sea level was approximately 50 m below present sea level at 11.62 kyr BP. This is approximately equal to the reconstruction of postglacial sea level for the western Pacific and from Barbados reef crest coral, given that the radiocarbon-based chronologies are subject to larger uncertainties over the last deglaciation, although it slightly deviates from the equivalent sea level curve

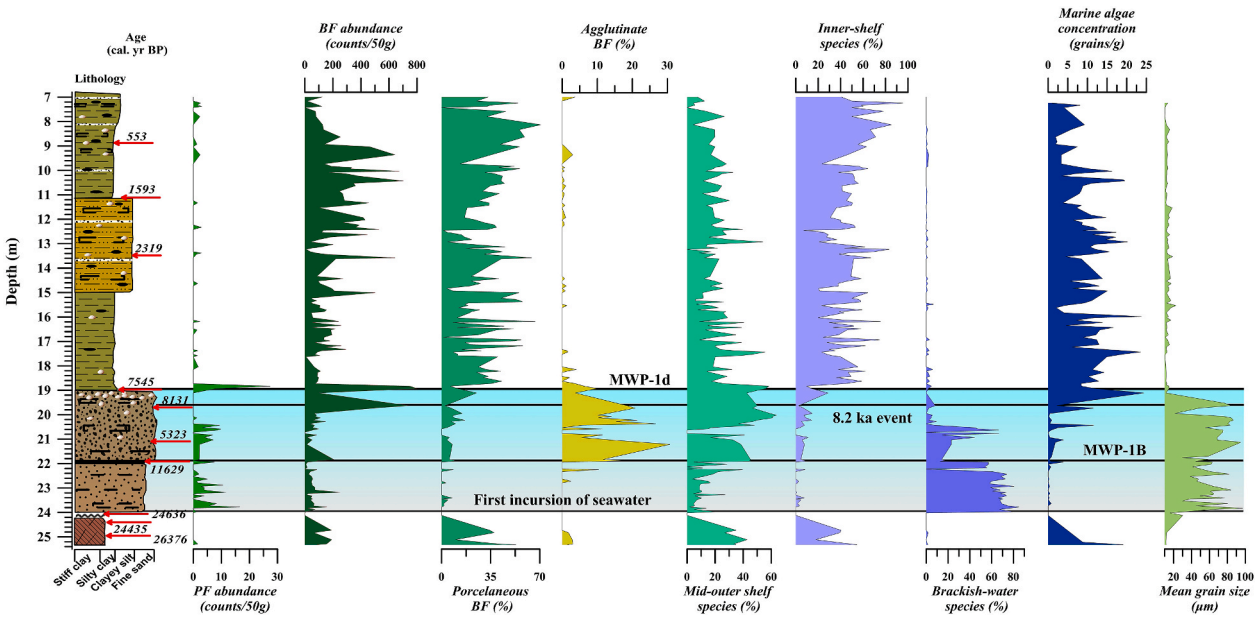

Fig. 5. Downcore variations in the abundance of both planktonic (PF) and benthic (BF) foraminifera, percentages of porcelaneous and agglutinated benthic foraminifera, and contents of mid-to outer-shelf, inner shelf and brackish-water benthic foraminifera species, the marine algae concentration and the mean grain size in core DC1. The legend for the lithology and sedimentary structure is the same as that in Fig. 2.

(Liu et al., 2004; Lambeck et al., 2014; Abdul et al., 2016) (Fig. 4). MWP-1B likely led to the rapid westward flooding of the ECS inner shelf, causing an energetic coastal environment with an increasing level of tidal inundation. After this rapid rise in sea level, the Yangtze-derived sediments were mostly trapped within the estuary due to the lack of a well-developed Chinese coastal current system (Hori et al., 2001; Xu et al., 2012), which serves to transport fine-grained sediment southward, limiting the input of sediment to the core site. Under such sediment-starved conditions, the energetic and erosive physical conditions induced by seawater flooding scoured away the older, fine-grained sediments, thus leaving the underlying coarse transgressive sands and abundant shell debris over the site (Liu et al., 2007a), which are well documented by our core lithology in the interval of 18.9–21.92 m (Fig. 2). The seawater flooding induced by MWP-1B has significantly changed the nearshore hydrological conditions along the ECS inner shelf, resulting in a nearshore subtidal environment with a substantial decline in the content of brackish-water species (Figs. 3 and 5).

5.1.3. *The postglacial transgression maximum*

The bottom of the mud wedge in our core is bounded by a shell fragment-rich basal layer on top of a fine-grained poorly graded sand section (Fig. 2). This shell-rich bed is a distinctive layer common in sediment cores from the Yangtze Delta area and represents the maximum flooding surface (MFS) during postglacial transgression (Liu et al., 2007a; Wang et al., 2010; Xu et al., 2016). The shell-rich layer is believed to have resulted from a limited sediment supply induced by a sudden sea-level rise (Wang et al., 2010). This abrupt rise in sea level likely caused the coastline to rapidly migrate landward, leading to a dramatic increase in accommodation space that overwhelmed the sediment supply and resulted in sediment starvation and abundant shell fragments over the core site. A^{14}C date from the top of the shell-rich layer in our core indicates that this surface formed at approximately 7.54 kyr BP (Fig. 2), which is coincident with the MFS records in the high-resolution seismic profiles from the subaqueous Yangtze Delta (Li et al., 2014; Xu et al., 2016). Also, this interface in our core correlates well with a prominent subsurface acoustic reflector overlain by a thick clinoform in the seismic profile across site DC1 (Fig. S2) (Liu et al., 2007a). Globally, the timing of this MFS overlaps with another abrupt sea-level rise event (termed CRE-3), previously documented in drowned coral reefs in the Caribbean-Atlantic region; this event raised sea level by 5–6 m over a few hundred years immediately following 7.6 kyr BP (Blanchon and Shaw, 1995). Although subsequent studies on various records have also suggested the possibility of this rapid sea-level rise (Blanchon et al., 2002; Bird et al., 2007; Yu et al., 2007; Tamura et al., 2009), its validity remains widely debated due to large differences in magnitude, rate and timing among individual studies.

In the western Pacific, this rapid flooding event (termed MWP-1d) was originally proposed by Liu et al. (2004) based on an extensive sea-level database. Subsequent investigations also found evidence for a rapid sea-level rise of 3–5 m at 7.5–7.0 kyr BP in Singapore (Bird et al., 2007) and in the Mekong River Delta, which allowed thick mangrove peat to be widely deposited in the Cambodian lowlands (Tamura et al., 2009). More recently, a rapid sea-level rise of 2 m from 7.4 to 7.2 kyr BP was recognized on the southern Yangtze Delta plain (Wang et al., 2012). This sea-level rise is also clearly evidenced by the sudden transition of the depositional environment to nearshore, shallow-sea conditions off the Yangtze mouth at approximately 7.4 kyr BP (Liu et al., 2010). Although the timing of these events identified in the above studies is slightly younger than that of the catastrophic rise event proposed by Blanchon and Shaw (1995), all of these records indicate the same magnitude of sea-level rise. We therefore believe that this abrupt sea-level rise event was responsible for this widespread stratigraphic signature, given the poorly constrained chronology in most studies and the potential regional expression of this sea-level jump. This prominent rise in sea level could have caused a substantive rearrangement of the environmental regime along the ECS coast, resulting in more stable inner shelf conditions since 7.54 kyr BP that facilitated the formation of a homogenous mud wedge over the core site (Figs. 2, 4 and 5).

5.2. *Sea-level signatures of the 8.2 kyr cooling event*

A specific sea-level jump during the early Holocene, associated with the 8.2 kyr cooling event, has been well presented by a wide variety of studies in various regions of the Northern Hemisphere (Törnqvist et al., 2004; Cronin et al., 2007; Kendall et al., 2008; Hijma and Cohen, 2010; Li et al., 2012). In our core, the prominent peak in benthic foraminiferal abundance at 8.13 kyr coincides well with a substantial increase in the percentages of inner shelf species, which were otherwise deficient after

the first incursion of seawater, suggesting abruptly deepening water and an intensive marine influence over the core site (Figs. 3 and 5). The sharp change is also roughly coincident with a remarkable peak in the marine algae concentration (Fig. 5), likely implying a sharp rise in sea level. Similar changes in coastal systems, such as an increased marine influence and shoreline retreat, have also been observed in deltaic sedimentary archives and incised-valley-fill systems from nearly all East Asian shelves, and these changes have been attributed to an abrupt sea-level rise at approximately 8.2 kyr (Hori and Saito, 2007; Tamura et al., 2009; Zhang et al., 2018). Moreover, this abrupt sea-level rise may also be responsible for both a notable hiatus and a sudden facies shift at approximately 8.4–8.2 kyr in cores from the Yellow Sea and the present subaqueous delta of the Yangtze River (Liu et al., 2007b, 2020). Thus, we infer that the sharp changes in our records, as described above, represent the sea-level jump at approximately 8.2 kyr.

There is broad consensus that the sea-level jump at approximately 8.2 kyr was induced by the final draining of proglacial Lake Agassiz-Ojibway in North America (Barber et al., 1999; Törnqvist and Hijma, 2012), which caused a few meters of sea-level rise over 100–200 yr at sites away from the lake (Li et al., 2012). Kendall et al. (2008) demonstrated by GIA modeling analysis that far-field sites could experience more significant signals associated with glacial lake drainage, which was probably a >3 m rise in sea level for tectonically stable Chinese coastal areas (Liu et al., 2020). This catastrophic meltwater release had immediate, large-scale atmospheric and oceanic impacts, weakening the AMOC and in turn triggering the subsequent cooling event that peaked at 8.2 kyr (Barber et al., 1999; Rohling and Pälike, 2005; Ellison et al., 2006; Cronin et al., 2007; Kleiven et al., 2008). In the Asian monsoon region, this abrupt cooling is clearly correlated with a prominent weakening event in the summer monsoon, as demonstrated in a large body of stalagmite $\delta^{18}O$ records (Fig. 4) (Wang et al., 2005, 2008; Fleitmann et al., 2007; Cheng et al., 2009; Liu et al., 2013). Under a weak summer monsoon, severely reduced rainfall would have resulted in lower river discharges, and thus, a limited local sediment supply would have been available to the ECS coastal system. Simultaneously, the abrupt landward migration of the river mouth induced by the concurrent sea-level jump would also have intensified sediment starvation over the core site. This sediment starvation and erosion exposed the coarse relict and transgressive sands on the seabed, as demonstrated by the peak mean grain size at approximately 8.13 kyr (Fig. 5). Accordingly, our data provide additional evidence for a widespread sea-level jump at ~8.2 kyr and also suggest that it was closely related to the 8.2 kyr cooling event, implying a widespread response of climate and sea level to catastrophic ice sheet collapse and freshwater release into the North Atlantic.

6. Conclusions

Our results suggest that the postglacial sedimentary sequence on the ECS inner shelf, resting on a late Pleistocene basement of stiff clay, developed with a three-stage abrupt transition of depositional environments triggered by the rapid deglacial rise in sea level. The first transition was related to the initial incursion of seawater to the inner shelf long after MWP-1A, as indicated by the sudden appearance of both planktonic foraminifera and typical benthic brackish-water species, which resulted in the formation of tidal flat environments over the core site. The subsequent shift in sedimentary facies at 11.62 kyr BP was associated with the initial flooding of the inner shelf, as shown by the sudden reduction in brackish-water species and an obvious increase in inner-shelf benthic species. This flooding was triggered by MWP-1B and converted the core site into a high-energy coastal environment. The prominent shift at 7.54 kyr BP corresponded to the maximum flooding of the inner shelf area and can also be attributed to a rapid rise in sea level, which led to the formation of the modern inner shelf environment over the core site, as demonstrated by the dominance of inner-shelf benthic species and the disappearance of brackish-water species. The abrupt rise in sea level at approximately 8.2 kyr BP is well documented by abrupt changes in the foraminiferal fauna and prominent peaks in the marine algae concentration. The notable connection between the sea-level jump at approximately 8.13 kyr and the synchronous weakening of the Asian monsoon also suggests that it was closely linked to the 8.2 kyr climate event.

Author statement

Fengming Chang conceived the presented idea, analyzed the data, prepared the original draft, wrote and edited the final manuscript. Tiegang Li acquired the financial support for the work leading to this publication, and supervised the findings of this work. Lihua Zhuang contributed to sample preparations, carried the parts of experiment, analyzed the data and aided in interpreting the results. Hanjie Sun contributed to the interpretation of the results, and worked on the manuscript. Zhifang Xiong providing critical feedback and helped shape the research and the manuscript. Rongtao Sun assisted with foraminifer analysis and interpreting the results.

Declaration of competing interest

The authors declare that they have no known competing financial interests or personal relationships that could have appeared to influence the work reported in this paper.

Acknowledgments

We thank two anonymous reviewers for their thoughtful suggestions that greatly improved the manuscript. We also thank the editors Steve Mitchell and Prof. French for their editorial handling of this manuscript. This work was supported by the Strategic Priority Research Program of the Chinese Academy of Sciences (No. XDB42000000), the National Special Project for Global Change and Air-Sea Interaction (No. GASI-GEOGE-04) and the National Natural Science Foundation of China (grants 42076051, 41830539, and 41876041). We are grateful to Q. Nan for helpful comments and revision of an earlier manuscript and to F. Qian for her laboratory assistance.

Appendix A. Supplementary data

Supplementary data to this article can be found online at https://doi.org/10.1016/j.ecss.2021.107423.

References

Abdul, N.A., Mortlock, R.A., Wright, J.D., Fairbanks, R.G., 2016. Younger Dryas sea level and meltwater pulse 1B recorded in Barbados reef crest coral *Acropora palmata*. Paleoceanography 31, 330–344. https://doi.org/10.1002/2015PA002847.

Barber, D.C., Dyke, A., Hillaire-Marcel, C., Jennings, A.E., Andrews, J.T., Kerwin, M.W., Bilodeau, G., McNeely, R., Southon, J., Morehead, M.D., Gagnon, J.M., 1999. Forcing of the cold event 8200 yr ago by catastrophic drainage of Laurentide lakes. Nature 400, 344–348. https://doi.org/10.1038/22504.

Bird, M.I., Fifield, L.K., Chang, C.H., Teh, T.S., Lambeck, K., 2007. An inflection in the rate of early mid-Holocene sea-level rise: a new sea-level curve for Singapore. Estuar. Coast Shelf Sci. 71, 523–536. https://doi.org/10.1016/j.ecss.2006.07.004.

Blanchon, P., Shaw, J., 1995. Reef drowning during the last deglaciation: evidence for catastrophic sea level rise and ice-sheet collapse. Geology 23, 4–8. https://doi.org/10.1130/0091-7613(1995)023.

Blanchon, P., Jones, B., Ford, D.C., 2002. Discovery of a submerged relic reef and shoreline off Grand Cayman: further support for an early Holocene jump in sea level. Sediment. Geol. 147, 253–270. https://doi.org/10.1016/S0037-0738(01)00143-9.

Braithwaite, C.J.R., 2016. Coral-reef records of Quaternary changes in climate and sea-level. Earth Sci. Rev. 156, 137–154. https://doi.org/10.1016/j.earscirev.2016.03.002.

Carlson, A.E., Clark, P.U., 2012. Ice sheet sources of sea level rise and freshwater discharge during the last deglaciation. Rev. Geophys. 50, RG4007. https://doi.org/10.1029/2011RG000371.

Chang, F., Li, T., Xiong, Z., Xu, Z., 2015. Evidence for sea level and monsoonally driven variations in terrigenous input to the northern East China Sea during the last 24.3 kyr. Paleoceanography 30, 642–658. https://doi.org/10.1002/2014PA002733.

Chen, Z., Stanley, D.J., 1995. Quaternary subsidence and river channel migration in the Yangtze delta plain, eastern China. J. Coast Res. 11, 927–945.
Cheng, H., Fleitmann, D., Edwards, R.L., Wang, X., Cruz, F.W., Auler, A.S., Mangini, A., Wang, Y., Kong, X., Burns, S.J., Matter, A., 2009. Timing and structure of the 8.2 kyr event inferred from δ18O records of stalagmites from China, Oman, and Brazil. Geology 37, 1007–1010. https://doi.org/10.1130/G30126A.
Clark, P.U., Marshall, S.J., Clarke, G.K.C., Hostetler, S.W., Licciardi, J.M., Teller, J.T., 2001. Freshwater forcing of abrupt climate change during the last glaciation. Science 293, 283–287. https://doi.org/10.1126/science.1062517.
Cronin, T.M., Voigt, P.R., Willard, D.A., Thunell, R.C., Halka, J., Berke, M., Pohlman, J., 2007. Rapid sea level rise and ice sheet response to 8200-year climate event. Geophys. Res. Lett. 34, L20603. https://doi.org/10.1029/2007GL031318.
Cuzzone, J.K., Clark, P.U., Carlson, A.E., Ullman, D.J., Rinterknecht, V.R., Milne, G.A., Lunkka, J., Wohlfarth, B., Marcott, S.A., Caffee, M., 2016. Final deglaciation of the Scandinavian Ice Sheet and implications for the Holocene global sea-level budget. Earth Planet Sci. Lett. 448, 34–41. https://doi.org/10.1016/j.epsl.2016.05.019.
Deschamps, P., Durand, N., Bard, E., Hamelin, B., Camoin, G., Thomas, A.L., Henderson, G.M., Okuno, J., Yokoyama, Y., 2012. Ice-sheet collapse and sea-level rise at the Bølling warming 14,600 years ago. Nature 483, 559–564. https://doi.org/10.1038/nature10902.
Dong, J., Li, A.C., Liu, X.T., Wan, S.M., Feng, X.G., Lu, J., Pei, W.Q., Wang, H.L., 2018. Sea-level oscillations in the East China Sea and their implications for global seawater redistribution during 14.0-10.0 kyr BP. Palaeogeogr. Palaeoclimatol. Palaeoecol. 511, 298–308. https://doi.org/10.1016/j.palaeo.2018.08.015.
Dutton, A., Carlson, A.E., Long, A.J., Milne, G.A., Clark, P.U., DeConto, R., Horton, B.P., Rahmstorf, S., Raymo, M.E., 2015. Sea-level rise due to polar ice-sheet mass loss during past warm periods. Science 349, aaa4019. https://doi.org/10.1126/science.aaa4019.
Ellison, C.R.W., Chapman, M.R., Hall, I.R., 2006. Surface and deep ocean interactions during the cold climate event 8200 years ago. Science 312, 1929–1932. https://doi.org/10.1126/science.1127213.
Fairbanks, R.A., 1989. 17,000-year glacio-eustatic sea level record: influence of glacial melting rates on the Younger Dryas event and deep-ocean circulation. Nature 342, 637–642. https://doi.org/10.1038/342637a0.
Fleitmann, D., Burns, S.J., Mangini, A., Mudelsee, M., Kramers, J., Villa, I., Neff, U., Al-Subbary, A.A., Buettner, A., Hippler, D., Matter, A., 2007. Holocene ITCZ and Indian monsoon dynamics 491 recorded in stalagmites from Oman and Yemen (Socotra). Quat. Sci. Rev. 26, 170–188. https://doi.org/10.1016/j.quascirev.2006.04.012.
Heaton, T.J., Köhler, P., Butzin, M., Bard, E., Reimer, R.W., Austin, W.E.N., Bronk Ramsey, C., Grootes, P.M., Hughen, K.A., Kromer, B., Reimer, P.J., Adkins, J., Burke, A., Cook, M.S., Olsen, J., Skinner, L.C., 2020. Marine20-the marine radiocarbon age calibration curve (0-55,000 cal BP). Radiocarbon 62. https://doi.org/10.1017/RDC.2020.68.
Hijma, M.P., Cohen, K.M., 2010. Timing and magnitude of the sea–level jump preluding the 8200 yr event. Geology 38, 275–278. https://doi.org/10.1130/G30439.1.
Hirabayashi, S., Yokoyama, Y., Suzuki, A., Miyairi, Y., Aze, T., 2017. Short-term fluctuations in regional radiocarbon reservoir age recorded in coral skeletons from the Ryukyu Islands in the north-western Pacific. J. Quat. Sci. 32, 1–6. https://doi.org/10.1002/jqs.2923.
Hori, K., Saito, Y., 2007. An early Holocene sea-level jump and delta initiation. Geophys. Res. Lett. 34, L18401. https://doi.org/10.1029/2007GL031029.
Hori, K., Saito, Y., Zhao, Q., Cheng, X., Wang, P., Sato, Y., Li, C., 2001. Sedimentary facies of the tide-dominated paleo-Changjiang (Yangtze) estuary during the last transgression. Mar. Geol. 177, 331–351. https://doi.org/10.1016/s0025-3227(01)00165-7.
Kendall, R.A., Mitrovica, J.X., Milne, G.A., Törnqvist, T.E., Li, Y.X., 2008. The sea-level fingerprint of the 8.2 kyr climate event. Geology 36, 423–426. https://doi.org/10.1130/G24550A.1.
Kleiven, H.F., Kisse, C., Laj, C., Ninnemann, U.S., Richter, T.O., Cortijo, E., 2008. Reduced North Atlantic deep water coeval with the glacial lake Agassiz freshwater outburst. Science 319, 60–64. https://doi.org/10.1126/science.1148924.
Lambeck, K., Rouby, H., Purcell, A., Sun, Y., Sambridge, M., 2014. Sea level and global ice volumes from the last glacial maximum to the Holocene. Proc. Natl. Acad. Sci. 111, 15296–15303. https://doi.org/10.1073/pnas.1411762111.
Langer, M.R., Thissen, J.M., Makled, W.A., Weinmann, A.E., 2013. The foraminifera from the bazaruto archipelago (Mozambique). Neues Jahrb Geol Paläontol Abh. 297, 155–170.
Lee, H.J., Chao, S.Y., 2003. A climatological description of circulation in and around the East China Sea. Deep-Sea Research II 50, 1065–1084. https://doi.org/10.1016/S0967-0645(03)00010-9.
Li, C.X., Wang, P., Sun, H.P., Zhang, J.Q., Fan, D.D., Deng, B., 2002. Late Quaternary incisedvalley fill of the Yangtze delta (China): its stratigraphic framework and evolution. Sediment. Geol. 152, 133–158. https://doi.org/10.1016/S0037-0738(02)00066-0.
Li, G.X., Li, P., Liu, Y., Q, L.L., M, Y.Y., Xu, J.S., Yang, Z.G., 2014. Sedimentary system response to the global sea level change in the East China Seas since the last glacial maximum. Earth Sci. Rev. 139, 390–405. https://doi.org/10.1016/j.earscirev.2014.09.007.
Li, Y.X., Törnqvist, T.E., Nevittand, J.M., Kohl, B., 2012. Synchronizing a sea-level jump, final Lake Agassiz drainage, and abrupt cooling 8200 years ago. Earth Planet Sci. Lett. 315–316, 41–50. https://doi.org/10.1016/j.epsl.2011.05.034.
Lie, H.J., Cho, C.H., 2016. Seasonal circulation patterns of the Yellow and East China Seas derived from satellite-tracked drifter trajectories and hydrographic observations. Prog. Oceanogr. 146, 121–141. https://doi.org/10.1016/j.pocean.2016.06.004.
Liu, J.P., Milliman, J.D., 2004. Reconsidering melt-water pulses 1A and 1B: global impacts of rapid sea-level rise. J. Ocean Univ. China 3 (3), 183–190. https://doi.org/10.1007/s11802-004-0033-8.
Liu, J.P., Milliman, J.D., Gao, S., Cheng, P., 2004. Holocene development of the Yellow river's subaqueous delta, north Yellow Sea. Mar. Geol. 209, 45–67. https://doi.org/10.1016/j.margeo.2004.06.009.
Liu, J.P., Xu, K.H., Li, A.C., Milliman, J.D., Velozzi, D.M., Xiao, S.B., Yang, Z.S., 2007a. Flux and fate of Yangtze River sediment delivered to the East China sea. Geomorphology 85, 208–224. https://doi.org/10.1016/j.geomorph.2006.03.023.
Liu, J., Saito, Y., Wang, H., Yang, Z., Nakashima, R., 2007b. Sedimentary evolution of the Holocene subaqueous clinoform off the shandong peninsula in the Yellow Sea. Mar. Geol. 236, 165–187. https://doi.org/10.1016/j.margeo.2006.10.031.
Liu, J., Saito, Y., Kong, X., Wang, H., Xiang, L., Wen, C., Nakashima, R., 2010. Sedimentary record of environmental evolution off the Yangtze River estuary, East China Sea, during the last ~13,000 years, with special reference to the influence of the Yellow River on the Yangtze River delta during the last 600 years. Quat. Sci. Rev. 29, 2424–2438. https://doi.org/10.1016/j.quascirev.2010.06.016.
Liu, J., Qiu, J., Saito, Y., Zhang, X., Nian, X., Wang, F., Xu, G., Xu, T., Li, M., 2020. Formation of the Yangtze Shoal in response to the post-glacial transgression of the paleo-Yangtze (Changjiang) estuary, China. Mar. Geol. 423, 106080 https://doi.org/10.1016/j.margeo.2019.106080.
Liu, Y.H., Henderson, G., Hu, C.Y., Mason, A.J., Charnley, N., Johnson, K.R., Xie, S.C., 2013. Links between the East asian monsoon and North Atlantic climate during the 8200 year event. Nat. Geosci. 6, 117–120. https://doi.org/10.1038/ngeo1708.
Meyssignac, B., Fettweis, X., Chevrier, R., Spada, G., 2017. Regional sea level changes for the twentieth and the twenty-first centuries induced by the regional variability in Greenland ice sheet surface mass loss. J. Clim. https://doi.org/10.1175/JCLI-D-16-0337.1.
Milne, G.A., Mitrovica, J.X., 2008. Searching for eustasy in deglacial sea-level histories. Quat. Sci. Rev. 27, 2292–2302. https://doi.org/10.1016/j.quascirev.2008.08.018.
Mitrovica, J.X., Tamisiea, M.E., Davis, J.L., Milne, G.A., 2001. Recent mass balance of polar ice sheets inferred from patterns of global sea-level change. Nature 409 (6823), 1026–1029. https://doi.org/10.1038/35059054.
Murray, J.W., 2006. Ecology and Applications of Benthic Foraminifera, 2006. Cambridge University Press, Cambridge, UK, p. 426pp.
Peltier, W.R., 2002. On eustatic sea level history: last Glacial Maximum to Holocene. Quat. Sci. Rev. 21 (1–3), 377–396. https://doi.org/10.1016/S0277-3791(01)00084-1.
Reimer, P., Austin, W.E.N., Bard, E., Bayliss, A., Blackwell, P.G., Bronk Ramsey, C., Butzin, M., Cheng, H., Edwards, R.L., Friedrich, M., Grootes, P.M., Guilderson, T.P., Hajdas, I., Heaton, T.J., Hogg, A.G., Hughen, K.A., Kromer, B., Manning, S.W., Muscheler, R., Palmer, J.G., Pearson, C., van der Plicht, J., Reimer, R.W., Richards, D.A., Scott, E.M., Southon, J.R., Turney, C.S.M., Wacker, L., Adolphi, F., Büntgen, U., Capano, M., Fahrni, S., Fogtmann-Schulz, A., Friedrich, R., Köhler, P., Kudsk, S., Miyake, F., Olsen, J., Reinig, F., Sakamoto, M., Sookdeo, A., Talamo, S., 2020. The IntCal20 Northern Hemisphere radiocarbon age calibration curve (0-55 cal kBP). Radiocarbon 62. https://doi.org/10.1017/RDC.2020.41.
Rohling, E.J., Pälike, H., 2005. Centennial-scale climate cooling with a sudden cold event around 8,200 years ago. Nature 434, 975–979. https://doi.org/10.1038/nature03421.
Smith, D.E., Harrison, S., Firth, C.R., Jordan, J.T., 2011. The early Holocene sea-level rise. Quat. Sci. Rev. 30, 1846–1860. https://doi.org/10.1016/j.quascirev.2011.04.019.
Stanford, J.D., Hemingway, R., Rohling, E.J., Challenor, P.G., Medina-Elizalde, M., Lester, A.J., 2011. Sea-level probability for the last deglaciation: a statistical analysis of far-field records Global Planet. Change 79, 193–203. https://doi.org/10.1016/j.gloplacha.2010.11.002.
Stuiver, M., Reimer, P.J., Reimer, R.W., 2021. Calib 8.2. http://calib.org. (Accessed 28 April 2021).
Sun, W., Zhang, H., Li, B., 1989. Study on paleomagnetism of cores DC1 and DC2 from East China sea. Mar. Sci. 5, 15–23.
Tamura, T., Saito, Y., Sieng, S., 2009. Initiation of the Mekong River delta at 8 kyr: evidence from the sedimentary succession in the Cambodian lowland. Quat. Sci. Rev. 28, 327–344. https://doi.org/10.1016/j.quascirev.2008.10.010.
Tian, S.Y., Yasuhara, M.M., Hong, Y.Y., Huang, H.H.M., Iwatani, H., Chiu, W.T.R., Mamo, B., Okahashi, H., Rasmussen, T.L., 2020. Deglacial–Holocene Svalbard paleoceanography and evidence of meltwater pulse 1B, 2020 Quat. Sci. Rev. 233, 106237. https://doi.org/10.1016/j.earscirev.2020.103249.
Törnqvist, T.E., Bick, S.J., González, J.L., Van der Borg, K., De Jong, A.F.M., 2004. Tracking the sea-level signature of the 8.2 ka cooling event: new constraints from the Mississippi Delta. Geophys. Res. Lett. 31, L23309. https://doi.org/10.1029/2004GL021429.
Törnqvist, T.E., Hijma, M.P., 2012. Links between early Holocene ice-sheet decay, sea-level rise and abrupt climate change. Nat. Geosci. 5, 601–606. https://doi.org/10.1038/ngeo1536.
Wang, P.X., Zhang, J.J., Min, Q.B., 1985. Distribution of foraminifera in surface sediments of the East China Sea. In: Wang, P.X. (Ed.), Marine Micropaleontology of China. China Ocean Press and Springer-Verlag, Beijing, pp. 34–69.
Wang, Y.J., Cheng, H., Edwards, R.L., He, Y.Q., Kong, X.G., An, Z.S., Wu, J.Y., Kelly, M.J., Dykoski, C.A., Li, X.D., 2005. The Holocene asian monsoon: links to solar changes and North Atlantic climate. Science 308, 854–857. https://doi.org/10.1126/science.1106296.
Wang, Y.J., Cheng, H., Edwards, R.L., Kong, X., Shao, X., Chen, S., Wu, J., Jiang, X., Wang, X., An, Z., 2008. Millennial- and orbital-scale changes in the East Asian monsoon over the past 224,000 years. Nature 451, 1090–1093. https://doi.org/10.1038/nature06692.

Wang, Z.H., Xu, H., Zhan, Q., Saito, Y., He, Z., Xie, J., Li, X., Dong, Y., 2010. Lithological and palynological evidence of late Quaternary depositional environments in the subaqueous Yangtze delta, China. Quat. Res. 73, 550–562. https://doi.org/10.1016/j.yqres.2009.11.001.

Wang, Z., Zhuang, C., Saito, Y., Chen, J., Zhan, Q., Wang, X., 2012. Early mid-Holocene sea-level change and coastal environmental response on the southern Yangtze delta plain, China: implications for the rise of Neolithic culture. Quat. Sci. Rev. 35, 51–62. https://doi.org/10.1016/j.quascirev.2012.01.005.

Wang, Z., Yang, S., Wang, Q., Zhang, Z., Zhang, X., Lan, X., Li, R., Huang, L., 2014. Late Quaternary stratigraphic evolution on the outer shelf of the Est China Sea. Continent. Shelf Res. 90, 5–16. https://doi.org/10.1016/j.csr.2014.04.015i.

Xu, K., Li, A., Liu, J.P., Milliman, J.D., Yang, Z., Liu, C.S., Kao, S.Ji, Wan, S., Xu, F., 2012. Provenance, structure, and formation of the mud wedge along inner continental shelf of the East China Sea: a synthesis of the Yangtze dispersal system. Mar. Geol. 291–294, 176–191. https://doi.org/10.1016/j.margeo.2011.06.003.

Xu, T., Wang, G., Shi, X., Wang, X., Yao, Z., Yang, G., Fang, X., Qiao, S., Liu, S., Wang, X., Zhao, Q., 2016. Sequence stratigraphy of the subaqueous Changjiang (Yangtze River) delta since the last glacial maximum. Sediment. Geol. 331, 132–147. https://doi.org/10.1016/j.sedgeo.2015.10.014.

Xue, C., 2014. Missing evidence for stepwise postglacial sea level rise and an approach to more precise determination of former sea levels on East China Sea Shelf. Mar. Geol. 348, 52–62. https://doi.org/10.1016/j.margeo.2013.12.004.

Yusuke, Y., Esat, T.M., Thompson, W.G., Thomas, A.L., Webster, J.M., Miyairi, Y., Sawada, C., Aze, T., Matsuzaki, H., Okuno, J.i., 2018. Rapid glaciation and a two-step sea level plunge into the Last Glacial Maximum. Nature 559, 603–607. https://doi.org/10.1038/s41586-018-0335-4.

Yoneda, M., Uno, H., Shibata, Y., Suzuki, R., Kumamoto, Y., Yoshida, K., Sasaki, T., Suzuki, A., Kawahata, H., 2007. Radiocarbon marine reservoir ages in the western Pacific estimated by pre-bomb molluscan shells. Nucl. Instrum. Methods Phys. Res., Sect. B 259, 432–437. https://doi.org/10.1016/j.nimb.2007.01.184.

Yu, S.Y., Berglund, B.E., Sandgren, P., Lambeck, K., 2007. Evidence for a rapid sea-level rise 7600 yr ago. Geology 35 (10), 891–894. https://doi.org/10.1130/G23859A.1.

Zang, Y.B., Li, S.Z., Guo, L.L., Suo, Y.H., Somerville, I.D., Zhao, S.J., Hui, G.G., Zhang, Y., Zheng, Q.L., 2016. Similarity and differentiation between the East China sea shelf basin and cenozoic basins in the northeast south China sea. Geol. J. 51, 304–317. https://doi.org/10.1002/gj.2826.

Zhang, X., Dalrymple, R.W., Lin, C.M., 2018. Facies and stratigraphic architecture of the late Pleistocene to early Holocene tide-dominated paleo-Changjiang (Yangtze River) delta. GSA Bulletin130 (3–4), 455–483. https://doi.org/10.1130/B31663.1.

Zong, Y., 2004. Mid-holocene sea-level highstand along the southeast coast of China. Quat. Int. 117, 5–67. https://doi.org/10.1016/S1040-6182(03)00116-2.